Structural studies of Sr_2GaSbO_6, Sr_2NiMoO_6, and Sr_2FeNbO_6 using pressure and temperature

2006 J. Phys.: Condens. Matter 18 8761

(http://iopscience.iop.org/0953-8984/18/39/008)

INSTITUTE OF PHYSICS PUBLISHING JOURNAL OF PHYSICS: CONDENSED MATTER

J. Phys.: Condens. Matter **18** (2006) 8761–8780 doi:10.1088/0953-8984/18/39/008

Structural studies of Sr_2GaSbO_6, Sr_2NiMoO_6, and Sr_2FeNbO_6 using pressure and temperature

Michael W Lufaso[1], René B Macquart[1], Yongjae Lee[2], Thomas Vogt[1] and Hans-Conrad zur Loye[1,3]

[1] Department of Chemistry and Biochemistry, University of South Carolina, 631 Sumter Street, Columbia, SC 29208, USA
[2] Department of Earth System Sciences, Yonsei University, Seoul 120749, Korea

E-mail: zurloye@mail.chem.sc.edu

Received 7 February 2006, in final form 13 August 2006
Published 11 September 2006
Online at stacks.iop.org/JPhysCM/18/8761

Abstract

Results from high-pressure synchrotron x-ray diffraction and high-temperature x-ray diffraction measurements on polycrystalline samples of the tetragonal perovskites Sr_2GaSbO_6, Sr_2NiMoO_6, and Sr_2FeNbO_6 are reported. A phase transition, where the unit cell changes symmetry from tetragonal to cubic, is observed for each compound at elevated temperatures. The phase transition changes the structure from one exhibiting an octahedral tilting distortion at ambient temperature to one that is untilted above the transition temperature. At elevated pressures the $c/\sqrt{2}a$ lattice parameter ratio increases, indicating that the magnitude of the octahedral tilting distortion is increasing as a function of pressure. In the pressure range studied, up to ~6 GPa, no phase transitions were observed.

1. Introduction

Ordered doubled perovskites have the general formula $A_2BB'O_6$, where A is typically a rare earth metal, alkali, or alkaline earth metal, and where B and B′ are typically transition metal or main group metal cations. The structural and compositional diversity of ordered double perovskites is well known and several hundred compounds have been reported in the literature to date [1]. Many of these compounds exhibit interesting physical properties, such as the room temperature colossal magnetoresistance in Sr_2FeMoO_6 [2]. The aristotype cubic ordered double perovskite may be described as consisting of corner-sharing $[BO_6]$ and $[B'O_6]$ octahedra, which alternate in all three directions. The A-site cations occupy the cavities formed by the corner-sharing octahedral network. Although many cubic ordered double perovskites are known, the majority of compositions crystallize in lower symmetry space groups due to

[3] Author to whom any correspondence should be addressed.

the occurrence of an octahedral tilting distortion in their structures [1]. These octahedral tilting distortions in perovskites have held the interest of many scientists over the years, where early work focused on the lattice dynamics and phase transitions of $SrTiO_3$ [3]. A convenient notation to describe these octahedral tilting distortions was later developed by Glazer [4]. More recent work consisting of a normal-mode analysis of octahedral tilting distortions in simple perovskites has shown that the tilting is in agreement with a condensing of a soft mode at the Brillouin zone boundary of an aristotype perovskite [5, 6]. Octahedral tilting in ordered perovskites has also been examined in several contributions [7–10], with a group-theoretical analysis being used to catalogue the structures of ordered double perovskites and to identify the group–subgroup relationships [11].

The difficulty of correctly assigning the space group symmetry of ordered double perovskites is sometimes caused by the high degree of pseudosymmetry and the sometimes weak reflections associated with the octahedral tilting distortions. This is particularly noteworthy in strontium containing perovskites, where the peak splitting may be subtle [12, 13]. Further evidence for this observation is provided by the three compounds that are the focus of this study, Sr_2NiMoO_6, Sr_2GaSbO_6, and Sr_2FeNbO_6, as each one has been described with several different unit cell symmetries. At ambient pressure and temperature Sr_2NiMoO_6 has been reported to be tetragonal with $a \approx c \approx 3.93$ Å [14], tetragonal with $a \approx 7.84$ Å and $c \approx 7.90$ Å [15, 16], and tetragonal with $a \approx 5.55$ Å and $c \approx 7.89$ Å [17, 18]. At ambient pressure and temperature, the lattice of Sr_2GaSbO_6 has been reported to be cubic with $a \approx 7.9$ Å [19], tetragonal with $a \approx c \approx 7.9$ Å [20], and more recently the structure was reported to crystallize in space group $I4/m$ (No 87) [21] with $a \approx 5.5$ Å and $c \approx 7.9$ Å [22]. At ambient pressure and temperature, the unit cell of Sr_2FeNbO_6 has been reported to be tetragonal with $a \approx c \approx 3.96$ Å [23, 24], cubic with $a \approx 3.99$ Å [25], orthorhombic with space group *Pbnm* (No 62) with $a \approx c \approx 5.60$ Å and $b \approx 7.96$ Å [26–28], and tetragonal with space group $I4/m$ with $a \approx 5.61$ Å and $c \approx 7.97$ Å [29].

Changes in temperature and pressure are known to cause structural phase transitions in ordered double perovskites. For example, pressure has been shown to induce structural phase transitions in several double perovskites, notable examples being Ba_2BiTaO_6 [30], Ba_2YTaO_6 [31], $Ba_2PrRu_{0.8}Ir_{0.2}O_6$ [32], and Ba_2BiSbO_6 [33]. Similarly, temperature has also been shown to exert an influence as, for example, in the case of Sr_2CoWO_6, which was found to undergo a phase transition from tetragonal (space group $I4/m$) to monoclinic symmetry (space group $P2_1/n$) upon cooling [34], while it was shown to undergo a phase transition to cubic symmetry (space group $Fm\bar{3}m$ (No 225)) upon heating [35] Interestingly, the crystal structure of Sr_2CoWO_6 has a space group symmetry (space group $I4/m$) that may be characterized as being intermediate, due to the existence of a phase transition to either higher or lower symmetry. These characteristics make the tetragonal perovskites model compounds with which to study the effect of pressure and temperature on structure. In this contribution, we report the results of *in situ* high-pressure and *in situ* high-temperature x-ray powder diffraction experiments performed on the tetragonal perovskites Sr_2NiMoO_6, Sr_2GaSbO_6, and Sr_2FeNbO_6.

2. Experimental details

Polycrystalline Sr_2NiMoO_6 and Sr_2FeNbO_6 were prepared by conventional solid state techniques, whereas Sr_2GaSbO_6 was prepared in a $SrCl_2$ flux with 2:1 flux to sample ratio. The samples were annealed with intermediate grinding and heating cycles until no more changes were evident in the diffraction peaks. Phase purity was established by powder x-ray diffraction using a Rigaku D/Max 2100 diffractometer. Approximately 2% of a secondary $SrMoO_4$ phase was observed in the synthesis of Sr_2NiMoO_6. *In situ* high-temperature x-ray powder diffraction

measurements with Cu Kα radiation (both Kα1 and Kα2 are present) were performed using a Rigaku D/MAX 2100 diffractometer with a Rigaku high-temperature attachment. The polycrystalline samples were mounted in a steel sample holder and the measurements were performed under flowing nitrogen. Diffraction data were collected from 15°–110° 2θ in 0.04° steps at each temperature interval. A sample was allowed to equilibrate at each temperature for 30 min before data collection commenced. Diffraction data analysis was performed using the FullProf software program [36]. A Thompson–Cox–Hastings pseudo-Voigt function was used to model the peak shapes in the angular range 15°–110° 2θ. The standard uncertainties are those reported by the software and may underestimate the uncertainty.

In situ high-pressure synchrotron x-ray powder diffraction experiments were performed using a diamond anvil cell (DAC) at the X7A beam-line at the national synchrotron light source (NSLS) at Brookhaven National Laboratory (BNL). Additional experimental set-up and detailed procedure may be found elsewhere [37]. The primary white beam from the bending magnet was monochromated to a wavelength of 0.622 45(4) Å using a channel-cut Ge(111) monochromator after a set of slits defining the beam size. A bent Si(111) monochromator is used to focus the original 0.5 mm × 15 mm rectangular beam to a ∼200 μm circular beam. Furthermore, a 200 μm pinhole is used to reduce any spread of the beam from the bent monochromator. The focused beam size is approximately 200 μm, compatible with but slightly larger than the size of the sample chamber, which has a diameter between 100 and 150 μm. A gas-proportional position-sensitive detector (PSD) was stepped in 0.25° intervals over the angular range of 5°–35° in 2θ with counting times of 50–100 s per step. The wavelength of the incident beam, PSD zero channel and PSD degrees/channel were determined from a CeO_2 standard (SRM 674). Polycrystalline samples were loaded into the DAC at ambient pressure and room temperature along with a few small ruby chips. A methanol–ethanol–water mixture with component ratio of 16:3:1 was used as the hydrostatic pressure-transmitting medium. The DAC is based on a modified Merrill–Bassett design and employs two diamonds with 0.5 mm diameter culets on tungsten-carbide supports. The x-rays are admitted by a 0.5 mm diameter circular aperture, and the exit beam leaves via a 0.5 mm × 3.0 mm rectangular tapered slit, oriented perpendicular to the horizontal plane of the diffractometer. The sample chamber is outfitted by a ≈60–80 μm diameter hole made using a spark-erosion method in the centre of a 250 μm thick stainless-steel gasket, pre-indented to 100 μm thickness before erosion. The DAC was placed on the second axis of the diffractometer, and the sample position was adjusted using a pre-centred microscope. The pressure at the sample was measured by detecting the shift in the R1 emission line of the included ruby chips. No evidence of nonhydrostatic conditions or pressure anisotropy were detected during our experiments, and the R1 peaks from three included ruby chips remained strong and sharp with deviations in the measured pressure of less than 0.2 GPa. All pressure-dependent diffraction patterns were collected at room temperature using a wavelength of 0.622 45(4) Å. Diffraction data analysis was performed using the EXPGUI interface of GSAS [38, 39]. A pseudo-Voigt function was used to model the peaks in the range employed in the refinements from 6° to 35° 2θ, excluding or modelling as the background the regions which contained strong Bragg peaks from the pressure cell gasket.

3. Results and discussion

Analysis of laboratory x-ray diffraction data show that Sr_2GaSbO_6, Sr_2NiMoO_6, and Sr_2FeNbO_6 crystallize in a tetragonal unit cell with $a \approx b \approx 5.6$ Å and $c \approx 7.9$ Å. Structure refinements were performed at ambient temperature and pressure with space group $I4/m$ for Sr_2GaSbO_6 and Sr_2NiMoO_6, which is in agreement with previous structural studies [18, 22]. We found that space group $I4/mcm$ (No 140) best described the symmetry of Sr_2FeNbO_6.

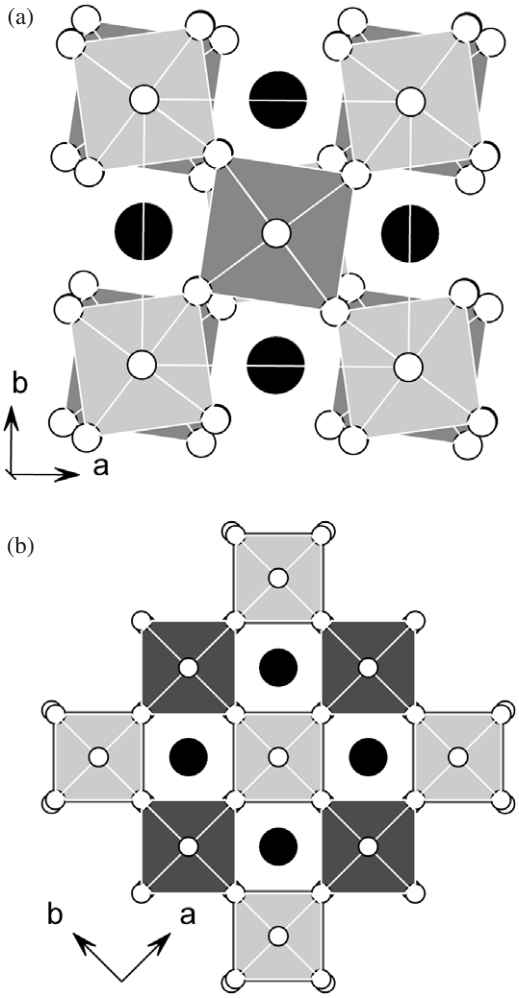

Figure 1. Crystal structure of Sr_2GaSbO_6 viewed along the *c*-axis in (a) space group $I4/m$ at ambient temperature and pressure and (b) space group $Fm\bar{3}m$ at 723 K. Large black spheres represent strontium and white spheres represent oxygen. Octahedra represent [GaO_6] (light grey) and [SbO_6] (dark grey).

The ordered double perovskites with space group $I4/m$ belong to a subgroup of the aristotype perovskite space group $Pm\bar{3}m$ (No 221), and may be obtained via the combination of the irreducible representations R_1^+ and R_4^+ for cation ordering and out of phase octahedral tilting, respectively [11]. The disordered perovskite with space group $I4/mcm$ belongs to a subgroup that may be obtained via the irreducible representation R_4^+ of the aristotype perovskite space group $Pm\bar{3}m$.

The crystal structure of Sr_2GaSbO_6 that was refined from the data set collected at 298 K is shown in figure 1(a). The structure is an ordered double perovskite with the GaO_6 and SbO_6 octahedra ordered in a rock-salt-like fashion. Along the [001] direction there is an anti-phase cooperative octahedral tilting distortion that may be described as $a^0a^0c^-$ using the Glazer notation [4]. In the generic $Sr_2BB'O_6$ structure, each succeeding [BO_6] or [$B'O_6$] octahedron is rotated about the [001] axis in an anti-phase manner such that there is a minimal difference

between the M–O1 and M–O2 and between the M′–O1 and M′–O2 bond distances in cases where there is no electronic driving force for octahedral distortion.

3.1. Sr_2GaSbO_6

Inspection of the x-ray diffraction data collected above ambient temperature revealed changes in the patterns that are noticeable in the high 2θ range. Figure 2 shows a portion of the x-ray diffraction pattern at temperatures up to 873 K. Near 94° 2θ there are three reflections, indexed as 136, 244, and 152 in space group $I4/m$. At higher temperature, these peaks begin to coalesce, and at 723 K become indexed as a single reflection 246. At large 2θ, one reflection results in two peaks visible in the diffraction pattern corresponding to both Cu Kα1 and Cu Kα2 wavelengths used in the experiment. Similarly, near 98° 2θ the 127, 145, 053, 343, and 251 peaks coalesce into a single peak near 723 K; increased peak overlap as the cell becomes more pseudocubic is the reason for the apparent increase in peak intensity. The temperature dependence of the high-angle region is shown in figure 2 (bottom). The changes in the diffraction peaks are easily visible at high angles. The systematic absences of the x-ray diffraction pattern at 723 K up to 873 K are indicative of a cubic space group with $a \approx 7.87$ Å. An ordered double perovskite with space group $Fm\bar{3}m$ was used in the Rietveld refinement [40, 41] of the data collected between 723–873 K. The crystal structure of Sr_2GaSbO_6 at 723 K is shown in figure 1(b). Notice the absence of an antiphase octahedral tilting distortion at 723 K.

The temperature dependence of the structural parameters and selected interatomic distances obtained from Rietveld refinements of Sr_2GaSbO_6 are given in table 1 for the structures refined in space group $I4/m$ and in table 2 for the structures refined in space group $Fm\bar{3}m$. At a temperature of 623 and 673 K, refinement of z for O1 was unstable and was, therefore, fixed at the value obtained at 573 K. The refined Ga–O and Sb–O bond lengths and valence sums are in agreement with those expected for Ga^{3+} and Sb^{5+}. The temperature dependence of the lattice parameters is shown in figure 5(a), where the a lattice parameter has been multiplied by $\sqrt{2}$ for ease of comparison. A slight contraction of the c-axis is evident, whereas the a lattice parameter changes more rapidly via a smooth increase with temperature. The more rapid change in the a lattice parameter is correlated to a change in the octahedral tilting, which does not affect the c-axis in the limit of rigid octahedra. The small slope change around 350 K is not attributed to any structural change; we consider the variation an artifact of the data collection and refinement procedure, i.e. correlations with sample displacement upon heating. The temperature dependence of the normalized unit cell volume is given in figure 6(a). A smooth trend in the change of volume suggests the possibility of a continuous phase transition from $I4/m$ to $Fm\bar{3}m$. A group theoretical analysis by Howard *et al* shows that the group–subgroup relation between $Fm\bar{3}m$ and $I4/m$ is allowed to be continuous [11].

3.2. Sr_2NiMoO_6

Inspection of the x-ray diffraction data of Sr_2NiMoO_6 collected above ambient temperature showed changes in the patterns that were visible in the high 2θ range that were similar to those found for Sr_2GaSbO_6. The phase transition occurs above 523 K, which is in agreement with the temperature of 503 K that was suggested previously [42]; the small difference between the transition temperatures may be related to different synthetic conditions or degree of cation ordering. The temperature dependence of the structural parameters and selected interatomic distances of Sr_2GaSbO_6 obtained from Rietveld refinements, shown in figure 3, are given in table 3 for the crystal structures refined in space group $I4/m$ and table 4 for the structures

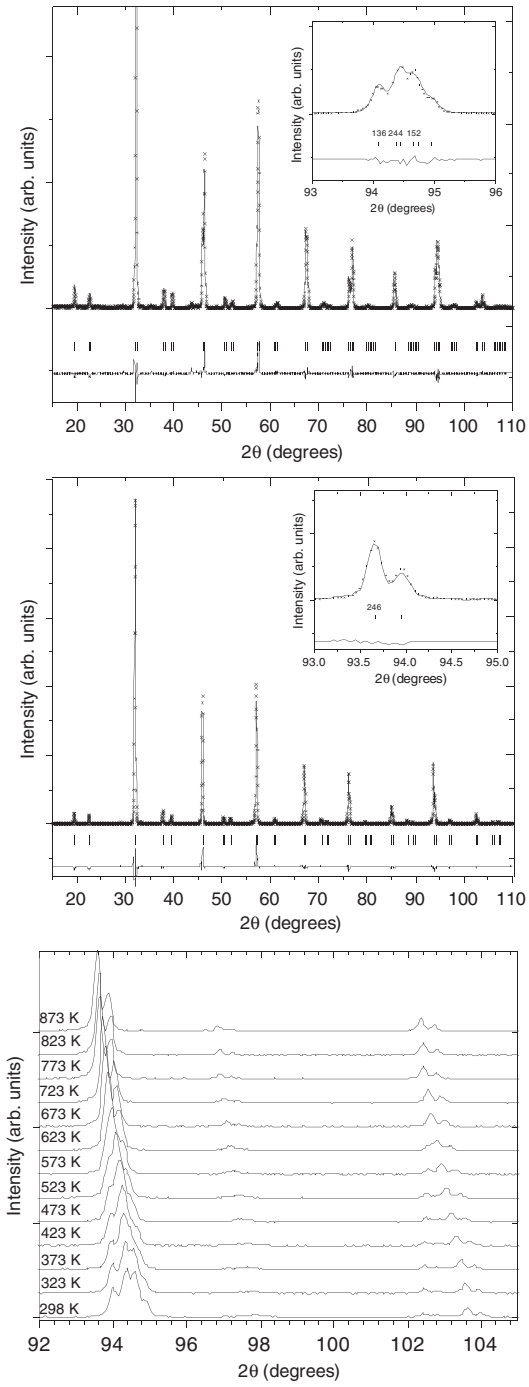

Figure 2. Rietveld refinement of Sr_2GaSbO_6 at 298 K (top) and 873 K (middle). Tick marks indicate allowed reflection positions in space group $I4/m$ (top) or $Fm\bar{3}m$ (middle). The difference pattern is given below the tick marks indicating allowed reflections. The inset shows the high-angle region near 95° 2θ. The high-angle region (bottom) of the x-ray diffraction pattern of Sr_2GaSbO_6 at increasing temperature from 298 to 873 K.

Table 1. Temperature dependence of the structural parameters and selected interatomic distances and angles of Sr_2GaSbO_6 obtained from Rietveld refinements. Atomic positions are Sr (0, 1/2, 1/4), Ga (0, 0, 0), Sb (1/2, 1/2, 0), O1 (0, 0, z), O2 (x, y, 0) in space group $I4/m$ (No 87).

	298 K	323 K	373 K	423 K	473 K	523 K	573 K	623 K	673 K
a (Å)	5.5411(1)	5.54318(6)	5.54727(8)	5.55171(6)	5.55652(8)	5.56147(8)	5.56642(7)	5.57176(8)	5.5767(2)
c (Å)	7.8982(2)	7.8975(1)	7.8967(1)	7.8958(2)	7.8949(2)	7.8950(2)	7.8928(2)	7.8910(2)	7.8901(5)
Vol. (Å^3)	242.511(7)	242.665(7)	242.999(7)	243.361(7)	243.754(7)	244.192(9)	244.559(6)	244.972(8)	245.37(2)
O1 z	0.239(2)	0.239(2)	0.238(2)	0.239(2)	0.238(3)	0.240(3)	0.239(4)	0.239(−)	0.239(−)
O2 x	0.205(2)	0.202(3)	0.203(2)	0.203(3)	0.200(3)	0.202(3)	0.204(3)	0.201(3)	0.200(3)
O2 y	0.277(2)	0.279(2)	0.276(2)	0.276(2)	0.280(3)	0.278(3)	0.276(3)	0.278(3)	0.279(3)
R_p (%)	10.0	9.83	9.94	9.89	9.50	9.79	9.09	9.36	9.79
R_{wp} (%)	15.1	14.8	15.2	15.0	14.7	14.9	14.4	14.6	14.8
χ^2	2.76	2.69	2.87	2.80	2.70	2.80	2.63	2.80	2.85
B_{iso} Å^2 (Sr)	1.32(4)	1.36(4)	1.46(4)	1.52(4)	1.56(4)	1.66(4)	1.78(4)	1.82(5)	1.90(5)
B_{iso} Å^2 (Ga)	0.66(7)	0.82(6)	0.81(7)	0.90(7)	0.84(5)	0.91(7)	0.85(7)	0.86(8)	1.01(8)
B_{iso} Å^2 (Sb)	1.10(5)	1.18(5)	1.24(5)	1.29(5)	1.32(5)	1.44(5)	1.39(5)	1.47(6)	1.54(5)
B_{iso} Å^2 (O)	0.6(2)	0.5(2)	0.5(2)	0.7(2)	0.5(2)	0.5(2)	0.8(2)	0.6(2)	0.8(2)
Ga–O2–Sb (deg)	163.6(6)	162.4(6)	163.4(6)	163.4(6)	161.8(8)	162.7(9)	163.6(9)	162.5(9)	162.0(9)
Ga–O1 (×2) Å	1.89(2)	1.89(1)	1.88(2)	1.89(2)	1.88(2)	1.89(2)	1.89(3)	1.89(−)	1.88(−)
Ga–O2 (×4) Å	1.91(1)	1.91(1)	1.90(1)	1.90(1)	1.91(1)	1.91(2)	1.91(2)	1.91(2)	1.91(2)
Sb–O1 (×2) Å	2.06(2)	2.06(1)	2.07(2)	2.06(2)	2.07(2)	2.05(2)	2.06(3)	2.06(−)	2.06(−)
Sb–O2 (×4) Å	2.05(1)	2.06(1)	2.06(1)	2.07(1)	2.07(1)	2.07(2)	2.07(2)	2.08(2)	2.08(2)

Table 2. Structural parameters and selected interatomic distances for Sr_2GaSbO_6 obtained from Rietveld refinement. Atomic positions are Sr (1/4, 1/4, 1/4), Ga (0, 0, 0), Sb (1/2, 0, 0), O1 (x, 0, 0) in space group $Fm\bar{3}m$ (No 225).

	723 K	773 K	823 K	873 K
a (Å)	7.891 69(6)	7.895 44(6)	7.899 52(6)	7.903 44(7)
Vol. (Å^3)	491.484(7)	492.185(7)	492.950(7)	493.682(7)
O1 x	0.2393(8)	0.2391(8)	0.2391(8)	0.2396(8)
R_p (%)	10.2	9.98	10.1	10.8
R_{wp} (%)	15.1	14.7	15.0	15.9
χ^2	2.98	2.87	3.01	3.41
B_{iso} Å^2 (Sr)	1.97(5)	2.03(5)	2.08(5)	2.17(5)
B_{iso} Å^2 (Ga)	1.25(2)	1.33(7)	1.31(7)	1.49(8)
B_{iso} Å^2 (Sb)	1.31(5)	1.27(5)	1.28(5)	1.35(5)
B_{iso} Å^2 (O)	2.4(2)	2.6(2)	2.6(2)	2.5(5)
Ga–O1 (×6) Å	1.888(6)	1.888(6)	1.889(6)	1.894(6)
Sb–O1 (×6) Å	2.057(6)	2.060(6)	2.061(6)	2.058(6)

refined in space group $Fm\bar{3}m$. The temperature dependences of the lattice parameters are given in figure 5(b). A contraction of the c lattice parameter is evident, whereas a smoothly increases with temperature. The temperature dependence of the unit cell volume is given in figure 6(b), which suggests the phase transition may be continuous. A study of Sr_2NiMoO_6 reported an anomaly in the heat capacity near 452 K [43]; however, no structural change is evident near that temperature. These results are in good agreement with those studies and the recent study of Sr_2NiMoO_6, where the same $I4/m$–$Fm\bar{3}m$ phase transition was found near 550 K [44].

3.3. Sr_2FeNbO_6

The ambient-temperature x-ray diffraction pattern of Sr_2FeNbO_6 was examined and could be indexed as tetragonal with $a \approx 5.60$ Å and $c \approx 7.96$ Å. Rietveld refinements were performed in space groups $I4/m$ and $I4/mcm$. The difference between the two structures is related to cation order: space group $I4/m$ allows for cation ordering between Fe and Nb, whereas space group $I4/mcm$ does not and, in fact, requires a cation disordered sublattice. Previous studies of Sr_2FeNbO_6 found partial cation order with a long range order of approximately 36% [45]. Refinements attempted in space group $I4/m$ at elevated temperatures were unstable. The difference between our results and those of Chmaissem *et al* may be related to different synthesis and annealing conditions. Inspection of the x-ray diffraction data of Sr_2FeNbO_6 collected above ambient temperature showed changes in the patterns that were visible in the high 2θ range and that were similar to those found for Sr_2NiMoO_6 and Sr_2GaSbO_6. The temperature dependence of the structural parameters and of selected interatomic distances of Sr_2FeNbO_6 obtained from Rietveld refinements, shown in figure 4, are given in table 5 for the crystal structures refined in space group $I4/mcm$ and in table 6 for the structures refined in space group $Pm\bar{3}m$. The temperature dependences of the lattice parameters are given in figure 5(c). Unlike both Sr_2NiMoO_6 and Sr_2GaSbO_6, where a contraction of the c lattice parameter is evident with an increase in temperature, the c-axis in Sr_2FeNbO_6 increases with temperature. The a lattice parameter also smoothly increases with temperature. The temperature dependence of the unit cell volume is given in figure 6(c). The temperature dependence of the (Fe/Nb)–O2–(Fe/Nb) bond angle is shown in figure 7. This angle increases

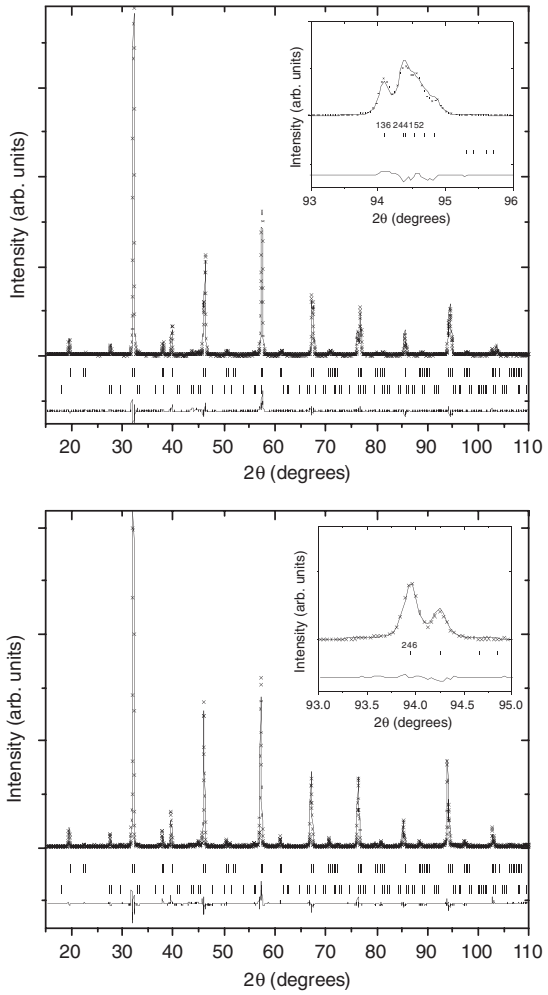

Figure 3. Rietveld refinement of Sr_2NiMoO_6 at 298 K (top) and 573 K (bottom). Tick marks indicate allowed reflection positions in space group $I4/m$ (top) or $Fm\bar{3}m$ (bottom). The top tick marks are for Sr_2NiMoO_6 and bottom tick marks are for $SrMoO_4$. The difference pattern is given below the tick marks. The inset shows the high-angle region near 94° 2θ.

as the structure approaches the phase transition, whereupon the (Fe/Nb)–O2–(Fe/Nb) angle is fixed by symmetry at 180°. An $I4/mcm$–$Pm\bar{3}m$ phase transition has also been observed in $La_{1-x}Sr_xMnO_3$ and $Pr_{1-y}Sr_yMnO_3$ [46].

3.4. High pressure

The high-pressure structural behaviour of simple perovskites (ABO_3) has been examined in terms of the relative compressibility of the AO_{12} and BO_6 polyhedra [47, 48]. If the AO_{12} is more compressible than the BO_6 polyhedra, the structure may become more distorted with pressure, which has been observed in $CaSnO_3$ [49]. If the AO_{12} is less compressible than the BO_6 polyhedra, the structure may become less distorted with pressure, which has been observed in $GdAlO_3$ and $GdFeO_3$ [48]. Furthermore, pressure may induce a phase transition to a higher

Table 3. Temperature dependence of the structural parameters and selected interatomic distances and angles of Sr_2NiMoO_6 obtained from Rietveld refinements. Atomic positions in fractional coordinates are Sr (0, 1/2, 1/4), Mo (0, 0, 0), Ni (1/2, 1/2, 0), O1 (0, 0, z), O2 (x, y, 0) in space group $I4/m$ (No 87).

	298 K	323 K	348 K	373 K	423 K	473 K	523 K
a (Å)	5.546 06(7)	5.548 29(7)	5.550 83(6)	5.553 29(6)	5.558 58(6)	5.564 20(6)	5.570 61(9)
c (Å)	7.8940(1)	7.8928(1)	7.8907(1)	7.8908(1)	7.8900(1)	7.8879(1)	7.8847(2)
Vol. (Å^3)	242.811(5)	242.968(5)	243.125(5)	243.345(5)	243.785(5)	244.213(6)	244.677(9)
O1 z	0.244(2)	0.244(2)	0.247(2)	0.247(2)	0.242(3)	0.243(5)	0.244(−)
O2 x	0.209(2)	0.210(3)	0.210(2)	0.206(3)	0.208(3)	0.205(3)	0.207(3)
O2 y	0.282(2)	0.287(2)	0.285(2)	0.285(3)	0.291(3)	0.286(3)	0.288(3)
R_p (%)	11.0	10.2	10.8	11.4	11.7	11.3	11.8
R_{wp} (%)	16.3	16.7	16.6	17.2	17.8	17.1	17.6
χ^2	2.72	2.85	2.84	3.01	3.26	2.94	3.13
B_{iso} Å^2 (Sr)	1.29(5)	1.12(4)	1.24(4)	1.13(4)	1.10(5)	1.20(5)	1.21(4)
B_{iso} Å^2 (Mo)	1.12(5)	1.15(5)	1.23(5)	1.23(5)	1.21(5)	1.33(5)	1.37(5)
B_{iso} Å^2 (Ni)	1.7(1)	1.7(1)	1.7(1)	1.9(1)	1.7(1)	2.0(1)	2.2(1)
B_{iso} Å^2 (O)	1.7(2)	1.7(2)	1.8(2)	2.3(3)	2.1(3)	2.1(3)	2.9(3)
Mo–O2–Ni (deg)	163.4(6)	162.5(7)	162.5(7)	162.0(7)	161(1)	161(1)	162(1)
Mo–O1 (×2) Å	1.93(2)	1.93(2)	1.94(2)	1.95(2)	1.91(2)	1.92(4)	1.92(−)
Mo–O2 (×4) Å	1.95(1)	1.97(1)	1.97(1)	1.95(2)	1.99(2)	1.97(2)	1.98(2)
Ni–O1 (×2) Å	2.02(2)	2.02(2)	2.00(2)	2.00(2)	2.04(2)	2.02(4)	2.02(−)
Ni–O2 (×4) Å	2.02(1)	2.00(1)	2.00(1)	2.02(2)	2.00(2)	2.02(2)	2.01(2)

Table 4. Structural parameters and selected interatomic distances for Sr_2NiMoO_6 obtained from Rietveld refinement at 573 K. Atomic positions in fractional coordinates are Sr (1/4, 1/4, 1/4), Mo (0, 0, 0), Ni (1/2, 0, 0), O1 (x, 0, 0) in space group $Fm\bar{3}m$ (No 225).

a (Å)	7.884 80(6)
Vol. (Å^3)	490.199(6)
O1 x	0.2438(9)
R_p (%)	12.3
R_{wp} (%)	18.3
χ^2	3.04
B_{iso} Å^2 (Sr)	1.07(5)
B_{iso} Å^2 (Mo)	1.02(5)
B_{iso} Å^2 (Ni)	2.9(1)
B_{iso} Å^2 (O)	3.5(2)
Mo–O1 (×6) Å	1.922(7)
Ni–O1 (×6) Å	2.020(7)

symmetry space group as was observed, for example, in $LaAlO_3$ [50], or it may induce a phase transition to a lower symmetry space group as was observed, for example, in Ba_2YTaO_6 [31]. If there is a phase transition present in the compounds of this study, then two possible pressure-induced phase transitions are from $I4/m$ to $P2_1/n$ or from $I4/m$ to $Fm\bar{3}m$, corresponding to the case where the structure becomes more distorted with pressure, and the case where it becomes less distorted with pressure, respectively.

The diffraction patterns of Sr_2NiMoO_6, Sr_2GaSbO_6, and Sr_2FeNbO_6 exhibited substantial peak broadening with increasing pressure that may be attributed to stresses at grain–grain contacts and antiphase boundaries resulting from imperfect cation order; a complete and

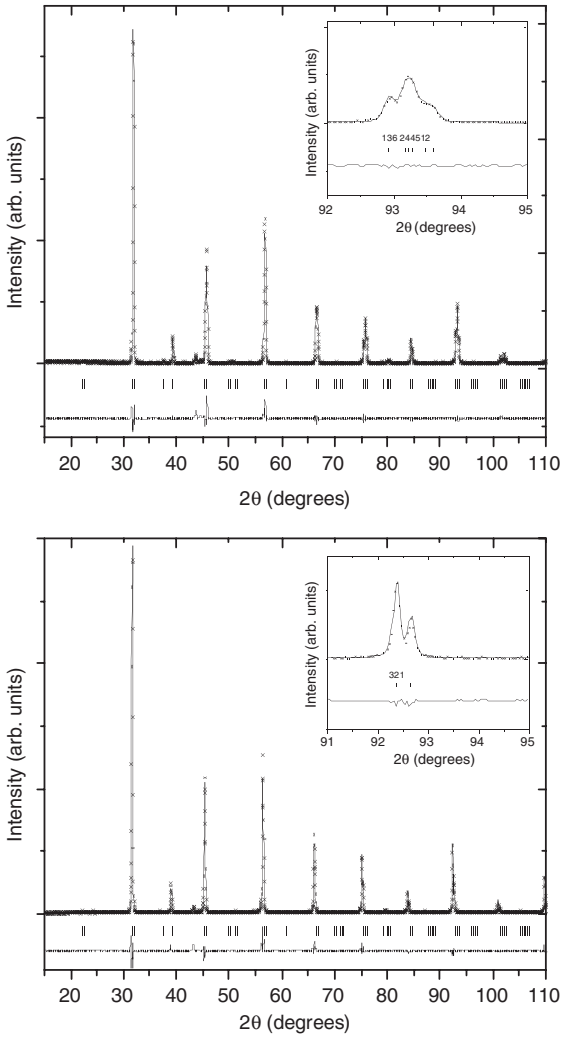

Figure 4. Rietveld refinement of Sr_2FeNbO_6 at 298 K (top) and 873 K (bottom). Tick marks indicate allowed reflection positions in space group $I4/mcm$ (top) or $Pm\bar{3}m$ (bottom). The difference pattern is given below the tick marks indicating allowed reflections. The inset shows the high-angle region near 93° 2θ.

selected regions of the diffraction pattern of Sr_2NiMoO_6 are shown in figures 8 and 9, respectively. Rietveld refinements of the structures were attempted, but resulted in large uncertainties in the atomic positions and unphysical changes in bond distances with changes in pressure. The small x-ray scattering cross section of oxygen compared to the heavy cations, the peak broadening that occurs as the pressure is increased, and the reduced number of reflections in the limited angular range, all prevent a full structure refinement. A Le Bail method analysis [51] was used to obtain the lattice parameters in the ordered double-perovskite structure, where the space group $I4/m$ was used for Sr_2NiMoO_6 and Sr_2GaSbO_6, while the space group $I4/mcm$ with a disordered cation arrangement was used for Sr_2FeNbO_6. A least-squares fit was used to determine the linear pressure dependence of the lattice parameters, which are shown in table 8 with lattice parameter units in Å and pressure in GPa. The

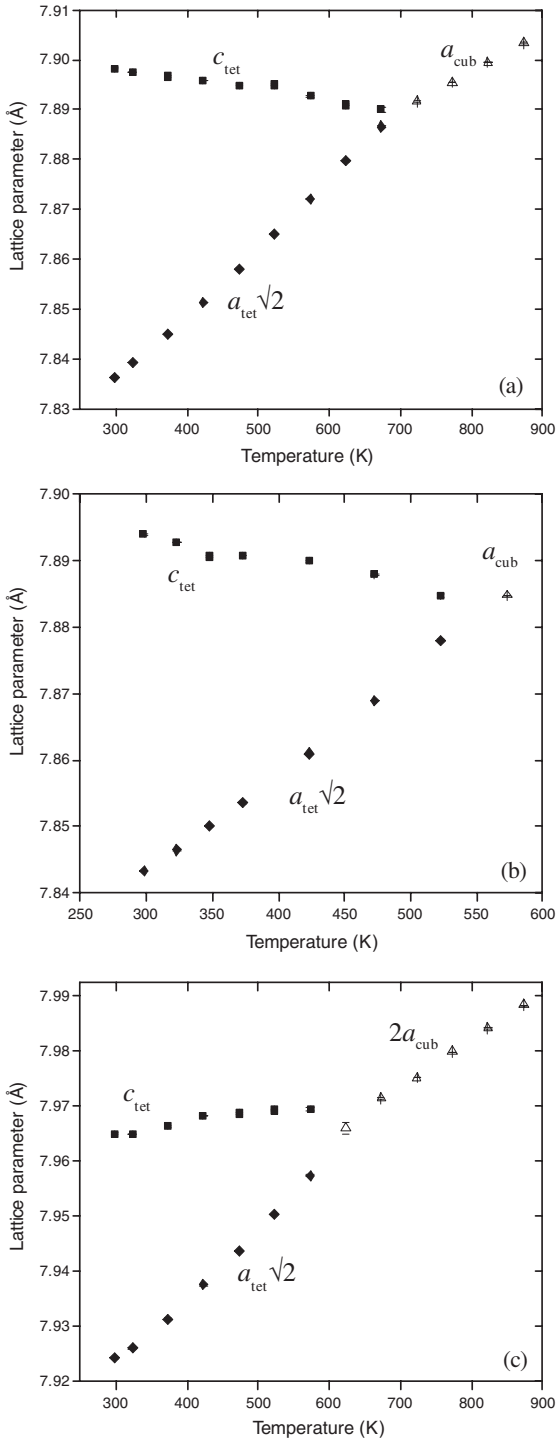

Figure 5. Temperature dependence of the lattice parameters of (a) Sr_2GaSbO_6, (b) Sr_2NiMoO_6, and (c) Sr_2FeNbO_6. Diamonds represent $\sqrt{2}a$ and squares represent c in the tetragonal cell, and triangles represent a for Sr_2GaSbO_6 and Sr_2NiMoO_6 or $2a$ for Sr_2FeNbO_6. Error bars are smaller than the symbol size.

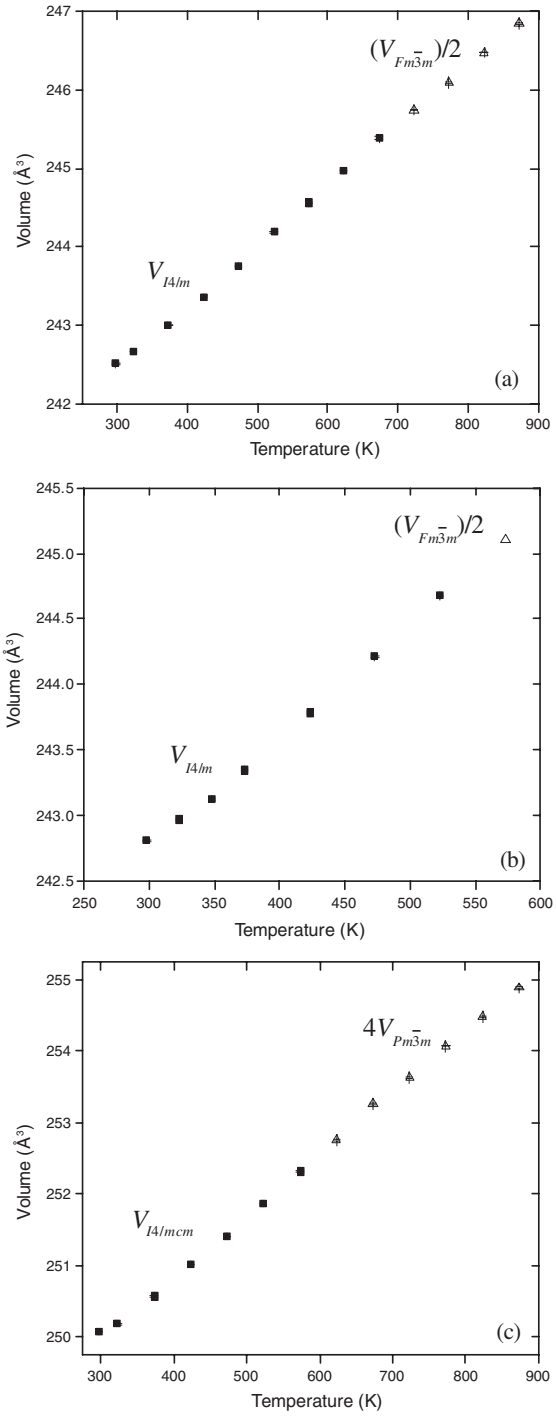

Figure 6. Temperature dependence of the unit cell volume of (a) Sr_2GaSbO_6, (b) Sr_2NiMoO_6, and (c) Sr_2FeNbO_6. Squares represent volume in space group $I4/m$, triangles volume/2 for Sr_2GaSbO_6 and Sr_2NiMoO_6 with space group $Fm\bar{3}m$, squares represent volume in space group $I4/mcm$, triangles volume $\times$ 4 for Sr_2FeNbO_6 with space group $Pm\bar{3}m$. Error bars are smaller than the symbol size.

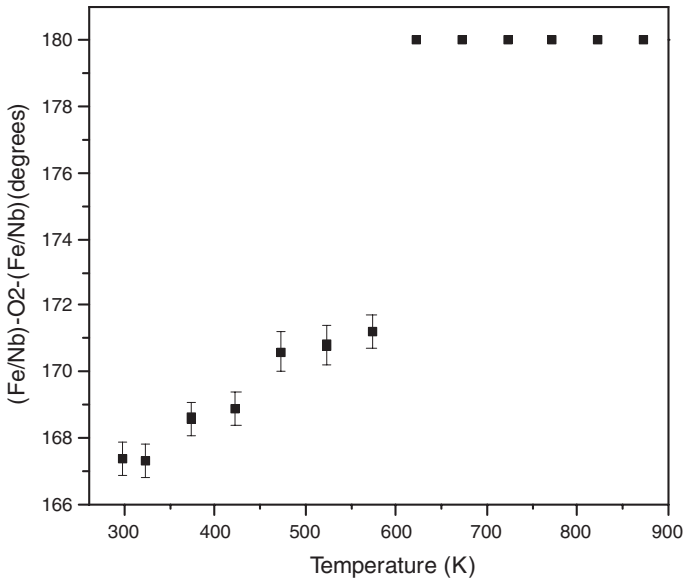

Figure 7. Temperature dependence of the (Fe/Nb)–O2–(Fe/Nb) bond angle of Sr_2FeNbO_6.

Table 5. Temperature dependence of the structural parameters and selected interatomic distances and angles of Sr_2FeNbO_6 obtained from Rietveld refinements. Atomic positions in fractional coordinates are Sr (0, 1/2, 1/4), Fe/Nb (0, 0, 0), O1 (0, 0, 1/4), O2 (x, $-x$, 0) in space group $I4/mcm$ (No 140).

	298 K	323 K	373 K	423 K	473 K	523 K	573 K
a (Å)	5.603 28(8)	5.604 53(6)	5.612 67(6)	5.612 67(6)	5.616 96(9)	5.621 78(6)	5.626 76(6)
c (Å)	7.9650(1)	7.9650(1)	7.9664(2)	7.9683(2)	7.9687(2)	7.9693(2)	7.9695(2)
Vol. (Å^3)	250.076(7)	250.185(7)	250.567(7)	251.017(7)	251.414(6)	251.865(9)	252.317(8)
O2 x	0.222(2)	0.222(1)	0.225(1)	0.226(1)	0.229(2)	0.230(2)	0.231(2)
R_p (%)	9.60	8.83	9.12	9.13	9.56	9.02	9.88
R_{wp} (%)	10.2	14.3	14.4	14.2	14.8	14.6	15.1
χ^2	1.89	1.94	1.96	1.95	2.16	2.11	2.17
B_{iso} Å^2 (Sr)	1.04(7)	1.28(7)	1.36(7)	1.53(8)	1.58(8)	1.81(7)	1.62(7)
B_{iso} Å^2 (Fe/Nb)	0.77(7)	0.96(7)	0.96(7)	0.99(7)	1.16(8)	1.00(7)	1.01(8)
B_{iso} Å^2 (O)	1.6(2)	1.6(2)	1.6(2)	1.6(2)	2.4(2)	2.1(2)	2.3(2)
Fe/Nb–O2–Fe/Nb (deg)	167.4(5)	167.3(5)	168.6(5)	168.9(5)	170.6(6)	170.8(6)	171.2(5)
Fe, Nb–O1 (×2) Å	1.991	1.991	1.992	1.992	1.992	1.992	1.992
Fe, Nb–O2 (×4) Å	1.993(8)	1.99(1)	1.993(8)	1.994(8)	1.99(1)	1.99(1)	2.00(1)

pressure dependence of the lattice parameter ratio $c/\sqrt{a}$ is shown in figure 10. The $c/\sqrt{a}$ ratio increases with an increase in pressure, which has been shown to correlate with an increase in the magnitude of the octahedral tilting distortion [31]. This implies that the structure becomes more distorted with pressure and that, therefore, the $I4/m$–$Fm\bar{3}m$ phase transition may be ruled out.

In a phase transition that also changes the octahedral tilting type, the resulting changes in the diffraction pattern may be weak and subtle and, therefore, difficult to separate from the background noise; the situation is further complicated by the peak broadening at higher pressures. A hypothetical crystal structure of a perovskite crystallizing with space group

Table 6. Structural parameters and selected interatomic distances for Sr_2FeNbO_6 obtained from Rietveld refinement. Atomic positions in fractional coordinates are Sr (1/2, 1/2, 1/2), Fe/Nb (0, 0, 0), O (1/2, 0, 0) in space group $Pm\bar{3}m$ (No 221).

	623 K	673 K	723 K	773 K	823 K	873 K
a (Å)	3.983 03(1)	3.985 73(4)	3.987 63(4)	3.989 94(4)	3.992 07(4)	3.994 18(4)
Vol. (Å^3)	63.189(1)	63.317(1)	63.408(1)	63.518(1)	63.620(1)	63.721
R_p (%)	11.4	10.1	10.5	9.5	10.0	9.84
R_{wp} (%)	16.4	14.6	15.5	14.8	14.7	14.7
χ^2	1.98	2.48	2.36	2.55	2.42	2.54
B_{iso} Å^2 (Sr)	1.45(8)	1.52(9)	1.27(7)	1.85(9)	1.55(9)	1.82(9)
B_{iso} Å^2 (Fe/Nb)	1.28(9)	0.86(9)	1.31(8)	1.08(9)	1.1(1)	1.1(1)
B_{iso} Å^2 (O)	3.7(2)	2.5(2)	3.8(2)	2.5(2)	2.6(2)	2.9(2)
Fe/Nb–O (×6) Å	1.991	1.992	1.994	1.994	1.996	1.997
Sr–O (×12) Å	2.816	2.818	2.819	2.821	2.823	2.824

Table 7. Pressure dependence of the lattice parameters and unit cell volume of Sr_2GaSbO_6 and Sr_2NiMoO_6.

Pressure (GPa)	a (Å)	c (Å)	Vol. (Å^3)
	Sr_2GaSbO_6		
0.9	5.5520(3)	7.9081(7)	243.77(3)
1.7	5.5385(3)	7.9079(10)	242.57(4)
3.2	5.5170(4)	7.8811(9)	239.88(4)
4.2	5.5150(3)	7.8814(13)	239.71(4)
5.1	5.4999(3)	7.8678(8)	237.99(3)
	Sr_2NiMoO_6		
0.4	5.5487(1)	7.9081(4)	243.47(1)
1.6	5.5400(3)	7.8973(8)	242.38(2)
2.6	5.5236(4)	7.883(1)	240.51(3)
4.4	5.5061(3)	7.8575(7)	238.22(3)
5.7	5.4959(3)	7.8575(9)	237.33(2)
	Sr_2FeNbO_6		
0.6	5.6085(2)	7.9732(5)	250.80(2)
1.4	5.6018(3)	7.9738(8)	250.21(3)
2.7	5.5839(5)	7.9578(14)	248.12(5)

$P2_1/n$ was generated using SPuDS [52]. The fractional coordinates were retained and the lattice parameters were refined. This approach has the advantage that it is a rapid method to generate the approximate peak intensities which result from the in-phase tilting and A-site displacements. The calculated peak intensities of the reflections allowed in $P2_1/n$ using this method are of a similar magnitude to the noise in the background. Although no obvious additional reflections were observed that could be associated with in-phase tilting or A-site cation displacements, these weak reflections could have been missed and, therefore, an analysis of the peak splitting was also undertaken. The peak near 22.4° 2θ was examined in detail, since it would be expected to split from a doublet of 024 and 132 in space group $I4/m$, to a quartet 204, $20\bar{4}$, 132, $13\bar{2}$ in space group $P2_1/n$. Figure 9(a) shows the pressure dependence of the

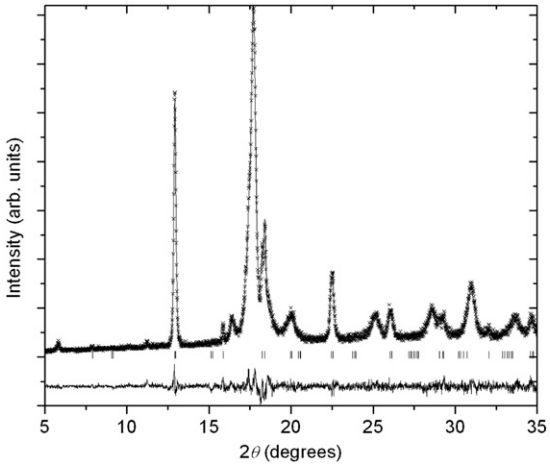

Figure 8. Pressure dependence of the synchrotron x-ray diffraction pattern of Sr_2NiMoO_6 at an applied pressure of 4.4(2) GPa. Tick marks indicate allowed reflection positions in space group $I4/m$. The difference pattern is given below the tick marks indicating the positions of allowed reflections. Contributions from the gasket were modelled as part of the background.

Table 8. Linear pressure dependence of the lattice parameters of Sr_2GaSbO_6, Sr_2NiMoO_6, and Sr_2FeNbO_6.

Sr_2GaSbO_6
$a(P) = 5.560(4)(1 - 2.11(20) \times 10^{-3}\ \mathrm{P})$
$c(P) = 7.919(1)(1 - 1.26(20) \times 10^{-3}\ \mathrm{P})$
Sr_2NiMoO_6
$a(P) = 5.553(2)(1 - 1.85(12) \times 10^{-3}\ \mathrm{P})$
$c(P) = 7.912(5)(1 - 1.32(17) \times 10^{-3}\ \mathrm{P})$
Sr_2FeNbO_6
$a(P) = 5.617(2)(1 - 2.14(24) \times 10^{-3}\ \mathrm{P})$
$c(P) = 7.981(1)(1 - 1.0(4) \times 10^{-3}\ \mathrm{P})$

region near 22.4° 2θ for Sr_2NiMoO_6. Although there are clearly two peaks at low pressures, the pressure-induced peak broadening obscures simple analysis of the peak splitting. Figure 9(b) shows the pressure dependence of the region near 25.8° 2θ for Sr_2NiMoO_6, which consists of the 224 and 040 reflections in space group $I4/m$, that would be expected to split into the $22\bar{4}$, 224, 040, and 400 reflections in space group $P2_1/n$. This region also has a clear doublet at low pressure; however, the substantial peak broadening again obscures an analysis of the peak splitting. Similar results were also found for both Sr_2GaSbO_6 and Sr_2FeNbO_6; therefore, these compounds all appear to retain tetragonal symmetry in the pressure range examined. It is possible that higher pressures may induce a phase transition and that the technique described above may be used to investigate phase transitions in perovskites. It is noteworthy that an analysis of energy dispersive x-ray diffraction measurements on Sr_2FeNbO_6 suggested that a structural or electronic phase transition occurred near 7.5 GPa based on changes in the electrical properties [53]. During data collection of Sr_2FeNbO_6 the gasket failed above 2.7 GPa, therefore only a limited range is presented.

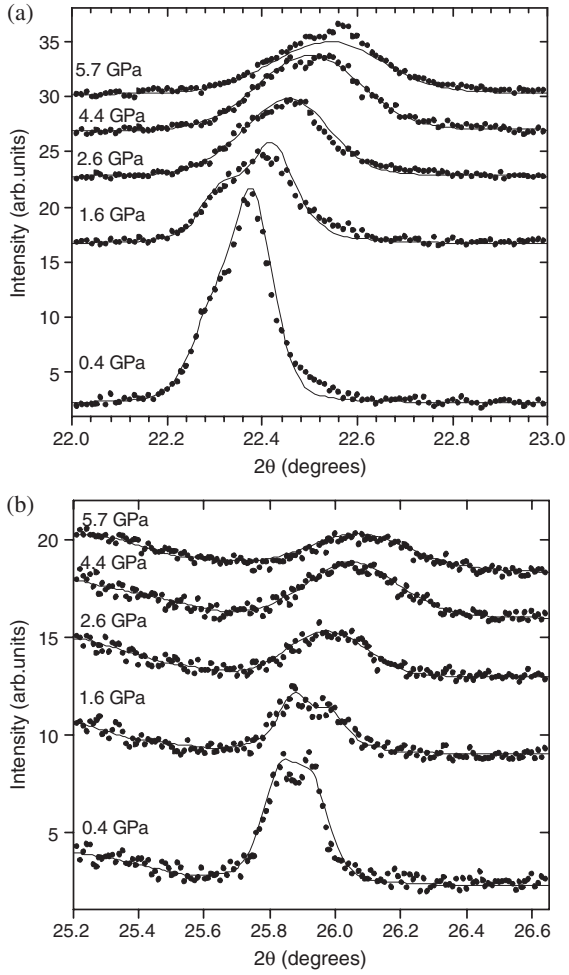

Figure 9. Pressure dependence of selected regions of the synchrotron x-ray diffraction pattern of Sr_2NiMoO_6.

Compressional moduli for the lattice of Sr_2NiMoO_6 are $K_{a0} = 171(12)$ GPa and $K_{c0} = 239(24)$ GPa and those for Sr_2GaSbO_6 are $K_{a0} = 140(16)$ GPa and $K_{c0} = 232(39)$ GPa. These were calculated using the unit cell volume obtained using $V_a = a \times a \times \sqrt{2}a$ and $V_c = c/\sqrt{2} \times c/\sqrt{2} \times c$ obtained from data given in table 7. It is noteworthy that the a-axis is more compressible than the c-axis for each of the three compounds. This observation may be explained by considering the ease of compression via both bond shortening and octahedral tilting along the a-axis, whereas, in contrast, bond shortening is the only compression mechanism possible along the c-axis in space group $I4/m$. The pressure dependence of the unit cell volume is shown in figure 11. Although the number of pressure points is small, we report approximate bulk moduli: Sr_2NiMoO_6 is 190(10) GPa, Sr_2GaSbO_6 is 164(18) GPa, and Sr_2FeNbO_6 is 187(27) GPa, and were obtained by fitting a second-order Birch–Murnaghan equation of state to the pressure dependence unit cell volume data, given in table 7, with a V_o of 244.0(2), 245.0(5), and 251.9(5) $Å^3$, respectively. The fitting procedure was done using the software program EOSFIT [54] using a fixed pressure derivative of the bulk modulus equal

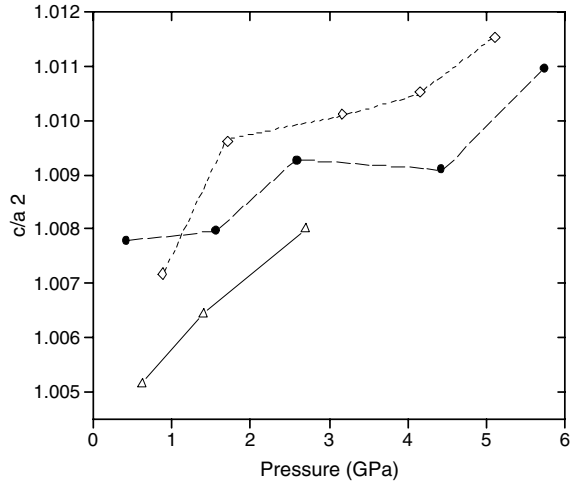

Figure 10. Pressure dependence of the lattice parameter ratio of (a) Sr_2GaSbO_6 (◇), (b) Sr_2NiMoO_6 (●), and (c) Sr_2FeNbO_6 (△). Short-dash, long-dash, and solid lines are guides to the eye for (a), (b), and (c), respectively. Error bars are smaller than the symbol size.

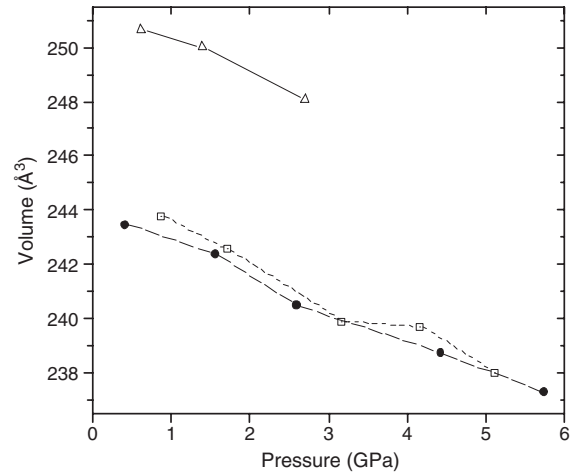

Figure 11. Pressure dependence of the unit cell volume of (a) Sr_2GaSbO_6 (□), (b) Sr_2NiMoO_6 (●), and (c) Sr_2FeNbO_6 (△). Short-dash, long-dash, and solid lines are guides to the eye for (a), (b), and (c), respectively. Error bars are smaller than the symbol size.

to $B' = 4$. The bulk moduli are comparable to that of another strontium containing double perovskite, $Sr_2TbRu_{0.3}Ir_{0.7}O_6$, whose bulk modulus is 196(10) GPa [55].

In conclusion, we have shown that the application of pressure induces a more rapid change in the a-lattice parameter than in the c-lattice parameter, which is indicative of an increase in the magnitude of the octahedral tilting distortion. There was no indication for a pressure induced phase transition up to 5.7 GPa in Sr_2NiMoO_6, Sr_2GaSbO_6, and to 2.7 GPa in Sr_2FeNbO_6. Their bulk moduli are similar to those of other Sr-containing ordered double perovskites. We have structurally characterized the temperature induced phase transition that Sr_2NiMoO_6, Sr_2GaSbO_6, and Sr_2FeNbO_6 exhibit near 523, 673, and 573 K, respectively. Upon heating, Sr_2NiMoO_6 and Sr_2GaSbO_6 undergo a phase transition from $I4/m$ to $Fm\bar{3}m$ and

Sr_2FeNbO_6 undergoes a phase transition from $I4/m$ to $Pm\bar{3}m$; concomitantly, the octahedral tilting distortion changes from an antiphase tilting ($a^0a^0c^-$) to an untilted form ($a^0a^0a^0$) in each case. The changes in cell parameters and unit cell volumes are indicative of a continuous phase transition.

Acknowledgments

Financial support from the Department of Energy through grant DE-FG02-04ER46122 and the National Science Foundation through grant DMR:0450103 is gratefully acknowledged. Work at Brookhaven is supported by the US Department of Energy, Division of Materials Sciences, under contract DE-AC02-98CH10886.

References

[1] Anderson M T, Greenwood K B, Taylor G A and Poeppelmeier K R 1993 *Prog. Solid State Chem.* **22** 197
[2] Kobayashi K L, Kimura T, Sawada H, Terakura K and Tokura Y 1998 *Nature* **395** 677
[3] Cowley R A 1964 *Phys. Rev.* **134** A981–97
[4] Glazer A M 1972 *Acta Crystallogr.* B **28** 3384
[5] Darlington C N W 2002 *Acta Crystallogr.* A **58** 66
[6] Darlington C N W 2002 *Acta Crystallogr.* A **58** 299
[7] Aleksandrov K S and Misyul S V 1981 *Sov. Phys.—Crystallogr.* **26** 612
[8] Woodward P M 1997 *Acta Crystallogr.* B **53** 32
[9] Woodward P M 1997 *Acta Crystallogr.* B **53** 44
[10] Bock O and Müller U 2002 *Acta Crystallogr.* B **58** 594
[11] Howard C J, Kennedy B J and Woodward P M 2003 *Acta Crystallogr.* B **59** 463
[12] Lufaso M W, Barnes P W and Woodward P M 2006 *Acta Crystallogr.* B **62** 384
[13] Barnes P W, Lufaso M W and Woodward P M 2006 *Acta Crystallogr.* B **62** 397
[14] Brixner L 1960 *J. Phys. Chem.* **64** 165
[15] Nomura S and Nakagawa T 1966 *J. Phys. Soc. Japan* **21** 1068
[16] Gagulin V V, Korchagina S K, Ivanova V V and Shevchuk Y A 2003 *Inorg. Mater.* **39** 625
[17] Teraoka Y, Wei M D and Kagawa S 1998 *J. Mater. Chem.* **8** 2323
[18] Martinez-Lope M J, Alonso J A and Casais M T 2003 *Eur. J. Inorg. Chem.* 2839
[19] Wittmann U, Rauser G and Kemmler-Sack S 1981 *Z. Anorg. Allg. Chem.* **482** 143
[20] Tauber A, Tidrow S C, Finnegan R D and Wilber W D 1996 *Physica* C **256** 340
[21] *International Tables for Crystallography* 2002 5th edn (Dordrecht: Kluwer–Academic)
[22] Barnes P W 2003 *PhD Thesis* Ohio State University, USA
[23] Kupriyanov M F and Fesenko E G 1961 *Kristallografiya* **6** 794
[24] Kupriyanov M F and Filip'ev V S 1963 *Kristallografiya* **8** 356
[25] Rodriguez R, Fernandez A, Isalgue A, Rodriguez J, Labarta A, Tejada J and Obradors X 1985 *J. Phys. C: Solid State Phys.* **18** L401–5
[26] Tezuka K, Henmi K, Hinatsu Y and Masaki N M 2000 *J. Solid State Chem.* **154** 591
[27] Kashima N, Inoue K, Wada T and Yamaguchi Y 2002 *Appl. Phys.* A **74** S805–7
[28] Zhao X, Yu R C, Yu Y, Li F Y, Liu Z X, Tang G D and Jin C Q 2004 *Mater. Sci. Eng.* B **111** 101
[29] Tao S, Canales-Vazquez J and Irvine J T S 2004 *Chem. Mater.* **16** 2309
[30] Wallwork K S, Kennedy B J, Zhou Q D, Lee Y and Vogt T 2005 *J. Solid State Chem.* **178** 207
[31] Lufaso M W, Macquart R B, Lee Y, Vogt T and zur Loye H-C 2006 *Chem. Commun.* 168
[32] Kennedy B J, Li L Q, Lee Y and Vogt T 2004 *J. Phys.: Condens. Matter* **16** 3295
[33] Lufaso M W, Macquart R, Lee Y, Vogt T and zur Loye H-C 2006 *J. Solid State Chem.* **179** 917
[34] Viola M C, Martinez-Lope M J, Alonso J A, Martinez J L, De Paoli J M, Pagola S, Pedregosa J C, Fernandez-Diaz M T and Carbonio R E 2003 *Chem. Mater.* **15** 1655
[35] Gateshki M, Igartua J M and Hernandez-Bocanegra E 2003 *J. Phys.: Condens. Matter* **15** 6199
[36] Rodriguez-Carvajal J 1990 FULLPROF: A program for Rietveld refinement and pattern matching analysis
[37] Vogt T, Schneider G, Hriljac J A, Yang G and Abell J S 2001 *Phys. Rev.* B **63** 220505
[38] Larson A C and von Dreele R B 1990 *General Structure Analysis System GSAS* Los Alamos National Laboratories
[39] Toby B H 2001 *J. Appl. Crystallogr.* **34** 210

[40] Rietveld H M 1967 *Acta Crystallogr.* **22** 151
[41] Rietveld H M 1969 *J. Appl. Crystallogr.* **2** 65
[42] Nomura S and Nakagawa T 1966 *J. Phys. Soc. Japan* **21** 1068
[43] Gunjikar V G, Ramachandran N and Keer H V 1982 *J. Indian Chem. Soc.* **59** 743
[44] Eriksson A K, Eriksson S-G, Ivanov S A, Knee C S, Eriksen J, Rundlöf H and Tseggai M 2006 *Mater. Res. Bull.* **41** 144
[45] Chmaissem O, Kruk R, Dabrowski B, Brown D E, Xiong X, Kolesnik S, Jorgensen J D and Kimball C W 2000 *Phys. Rev.* B **62** 14197
[46] Chmaissem O, Dabrowski B, Kolesnik S, Mais J, Jorgensen J D and Short S 2003 *Phys. Rev.* B **67** 094431
[47] Zhao J, Ross N L and Angel R J 2004 *Acta Crystallogr.* B **60** 263
[48] Ross N L, Zhao J and Angel R J 2004 *J. Solid State Chem.* **177** 3768
[49] Zhao J, Ross N L and Angel R J 2004 *Phys. Chem. Minerals* **31** 299
[50] Zhao J, Ross N L and Angel R J 2004 *J. Phys.: Condens. Matter* **16** 8763
[51] Le Bail A, Duroy H and Fourquet J L 1988 *Mater. Res. Bull.* **23** 447
[52] Lufaso M W and Woodward P M 2001 *Acta Crystallogr.* B **57** 725
[53] Zhao X, Yu R C, Yao L D, Li F Y, Liu Z X, Bao Z X, Li X D, Li Y C, Ma M N, Liu J, Tang G D and Jin C Q 2004 *J. Phys.: Condens. Matter* **16** 1299
[54] Angel R J 2001 *Equations of State Reviews in Mineralogy and Geochemistry* vol 41 ed R M Hazen and R T Downs, (Chantilly, VA: Mineralogical Society of America) pp 35–60
[55] Zhou Q, Kennedy B J, Wallwork K S, Elcombe M M, Lee Y and Vogt T 2005 *J. Solid State Chem.* **178** 2282